BOREAL ENVIRONMENT RESEARCH 31: 75–89
ISSN 1797-2469 (online)
Helsinki 31 August 2026

Scalability of climate change in Estonia with the level of global warming

Erko Jakobson[1)]*, Liisi Jakobson[1)], Hannes Keernik[2)], Andres Luhamaa[2)], Piia Post[2)], Margit Aun[2)] and Velle Toll[2)]

[1)] Tartu Observatory, Faculty of Science and Technology, University of Tartu, Observatooriumi 1, 61602 Tõravere, Estonia
[2)] Institute of Physics, Faculty of Science and Technology, University of Tartu, W. Ostwaldi 1, 50411 Tartu, Estonia
*corresponding author's e-mail: erko.jakobson@ut.ee

Received 7 Nov. 2025, final version received 14 Apr. 2026, accepted 28 May 2026

Jakobson E., Jakobson L., Keernik H., Luhamaa A., Post P., Aun M. & Toll V. 2026: Effect of ice cover on wave statistics and wave-driven processes in the northern Baltic Sea. *Boreal Env. Res.* 31: 75–89.

We analysed climate projections for Estonia using a global warming level (GWL) based approach and the CMIP6 ensemble. We quantified regional responses of temperature, precipitation, and wind-speed related indicators as linear functions of GWL. In general, temperature-related indicators scale well with GWL. Annual mean air temperature in Estonia rises by 1.5°C per 1°C of global warming (winter +1.9; summer +1.3). However, only a subset of changes in precipitation and wind-related indicators scale with GWL. Annual precipitation increases by 31 mm (4.6%) per 1°C of global warming, and extreme precipitation intensifies. Mean wind speeds decline slightly in summer and autumn, while changes in wind extremes remain uncertain. The limited scalability of regional changes in precipitation and wind-related indicators reflects uncertain atmospheric circulation responses to global warming.

Introduction

Climate change is creating growing challenges for societies worldwide, increasing the need for reliable climate projections to support adaptation. The knowledge of changes in regional climate is essential for updating adaptation strategies, adjusting infrastructure design standards, and informing long-term environmental policies in sectors such as agriculture, energy infrastructure, forestry, water management, and urban planning (Cradock-Henry *et al.* 2020, Snyder *et al.* 2024). Recently, presenting regional climate change information as a function of Global Warming Level (GWL, defined in Statistical methods section) has become the state of the art (Stammer *et al.* 2018, IPCC 2021: AR6 Ch10, Lafferty and Sriver 2023, Da Silva and Haerter 2025, Ruosteenoja and Jylhä 2025).

Compared to scenario-dependent approaches, the GWL-based approach provides a more flexible basis for climate change assessments (IPCC 2021: AR6 Ch1). In the case of the GWL-based approach, each model contributes data once it reaches a given warming threshold, independent of its emissions scenario or climate sensitivity, thereby decoupling regional projections from scenario-specific assumptions. For example, Becsi and Formayer (2024) showed for Austria that regional warming increments between

Editor in charge of this article: Veli-Matti Kerminen
https://doi.org/10.60910/ber2026.tmqs-yb90

GWLs remain relatively constant, independent of emission scenario and even of the chosen global climate model ensemble. Moreover, the GWL-based approach allows to analyse regional changes irrespective when in time given global warming level is reached.

Importantly, the GWL-based approach helps to reduce biases associated with so-called "hot models", which project stronger warming than the assessed likely range (Hausfather *et al.* 2022). Alternatively, the hot models could be screened out based on the elevated Equilibrium Climate Sensitivity (ECS) or Transient Climate Response (TCR) values (Hausfather *et al.* 2022). Previous studies have shown that GWL-based approaches allow for the inclusion of the full Coupled Model Intercomparison Project Phase 6 (CMIP6) ensemble while maintaining policy relevance and physical robustness (Hausfather *et al.* 2022, Goldenson *et al.* 2023).

Recent evaluations make a case for the use of the whole global model ensemble for analysing regional changes in Northern Europe, noting that some high-ECS models demonstrate strong performance in simulating historical climate variability in the region (Goldenson *et al.* 2023, Palmer *et al.* 2023). Importantly, for multiple aspects of regional climate change in the Baltic Sea region, different climate models give quite different results (Christensen and Kjellström 2018). Some of these conflicting results are likely explained by different climate sensitivities of individual global climate models. Some inter-model differences are likely explained by the uncertain response of the large-scale atmospheric circulation to global warming (Zappa and Shepherd 2017), unforced internal climate variability (Hawkins and Sutton 2009, Deser and Phillips 2023), different physical parameterizations (García-Díez *et al.* 2015) and horizontal resolutions (Strandberg and Lind 2021) in different models, among other possible explanations.

Atmospheric circulation responses to global warming are diverse (Shepherd 2014). For example, climate model projections of changes in cyclonic activity in specific subregions of the Baltic Sea region diverge: some models predict less, while others predict more cyclonic activity with global warming in the region (Shepherd 2014, Zappa and Shepherd 2017). Taking an example of cold season precipitation in the Baltic Sea region, the stronger the global warming, the stronger the intensification of the atmospheric water cycle (IPCC 2021, WGI Ch. 8), but at the same time, less/more cyclonic activity would also mean less/more precipitation. This illustrates why, based on scenario-following projections alone, it is challenging to distinguish whether the differences between projections of individual climate models are caused by different levels of global warming, differences in atmospheric circulation responses (Zappa and Shepherd 2017, Zappa 2019) or other reasons (Hawkins and Sutton 2009, Deser and Phillips 2023).

Using the GWL-approach, model diversity of regional projections can be analysed at a fixed level of warming. Here, we scale the climate change in Estonia with the level of global warming using the CMIP6 ensemble (Eyring *et al.* 2016) to quantify the most robust responses in the climate of Estonia. This enables us to tease out other reasons for inter-model differences, including diverging circulation responses. As Estonia is a relatively small region, we also analyse regional changes in the Baltic Sea region for improved interpretation.

Material and methods

Selection of CMIP6 models

We use CMIP6 global climate models' projections used in the Copernicus Interactive Climate Atlas (C3S Atlas) (CSIC 2023). There were 39 models featured in the Atlas. We excluded models with the 360-day calendar format due to unification problems with other models. In total, we included 31 models (Table 1) available in the Amazon AWS CMIP6 archive (Amazon Web Services Open Data Program 2025).

The CMIP6 data used in this study were not bias-corrected. The use of raw CMIP6 model output is consistent with the approach adopted in IPCC AR6 and the IPCC Interactive Atlas, where regional changes are assessed using anomalies rather than bias-adjusted data. Our study focuses on scaling relationships between regional climate indicators and global warming levels (GWLs), based on regression slopes within each model. Because the analysis is based on relative changes with respect to the pre-industrial baseline and the slope of change per °C of global warming, systematic mean-state biases do not directly affect the estimated scaling coefficients for parameters like temperature, precipitation, and wind. However, bias-corrected data can be more relevant for threshold-based indices, where absolute values relative to fixed thresholds determine event counts (e.g., frost- and ice-related day counts, tropical nights, and heating degree days). In such cases, a warm or cold bias may shift the baseline frequency of threshold exceedances and can influence absolute counts, particularly when the climate is close to the threshold. In this study, we interpret threshold-based results primarily in terms of the direction of change and sensitivity to GWL, rather than as impact-assessment-ready absolute frequencies.

To evaluate whether outlier models with unusually high or low climate sensitivity systematically bias regional projections, we tested the influence of including climate models with a transient climate response (TCR) outside the likely (66% likelihood) range of 1.4–2.2°C and equilibrium climate sensitivity (ECS) outside the 2.5–4°C range (Hausfather *et al.* 2022). Model-specific ECS and TCR values are obtained from the AR6 supplementary materials (Smith *et al.*

Table 1. Equilibrium Climate Sensitivity (ECS) and Transient Climate Response (TCR) for CMIP6 models used in this study. For testing the influence of including all models irrespective of their climate sensitivity, models are grouped into Normal (N), Hot (H) and Cold (C), having N criteria 2.5–4 °C for ECS and 1.4–2.2 °C for TCR (Hausfather *et al.* 2022). In Hot models, ECS and/or TCR are higher than the N criteria, and in Cold models, ECS and/or TCR are lower than the N criteria.

Model	ECS °C	TCR °C	ECS	TCR
ACCESS-CM2_r1i1p1f1	4.72	2.10	H	N
AWI-CM-1-1-MR_r1i1p1f1	3.16	2.06	N	N
BCC-CSM2-MR_r1i1p1f1	3.04	1.72	N	N
CanESM5_r1i1p1f1	5.62	2.74	H	H
CAMS-CSM1-0_r2i1p1f1	2.29	1.73	C	N
CESM2-WACCM_r1i1p1f1	4.75	1.98	H	N
CMCC-CM2-SR5_r1i1p1f1	3.52	2.09	N	N
CMCC-ESM2_r1i1p1f1	3.57	1.97	N	N
CNRM-CM6-1_r1i1p1f2	4.83	2.14	H	N
CNRM-CM6-1-HR_r1i1p1f2	4.28	2.48	H	H
CNRM-ESM2-1_r1i1p1f2	4.76	1.86	H	N
EC-Earth3-AerChem_r1i1p1f1	3.90	2.10	N	N
EC-Earth3-CC_r1i1p1f1	4.23	2.30	H	H
EC-Earth3-Veg-LR_r1i1p1f1	4.31	2.62	H	H
FGOALS-f3-L_r1i1p1f1	3.00	1.94	N	N
FGOALS-g3_r1i1p1f1	2.88	1.54	N	N
GFDL-ESM4_r1i1p1f1	2.60	1.60	N	N
IITM-ESM_r1i1p1f1	2.37	1.71	C	N
INM-CM4-8_r1i1p1f1	1.83	1.33	C	C
INM-CM5-0_r1i1p1f1	1.92	1.41	C	N
IPSL-CM5A2-INCA_r1i1p1f1	3.81	1.93	N	N
IPSL-CM6A-LR_r1i1p1f1	4.56	2.32	H	H
KIOST-ESM_r1i1p1f1	3.36	NA	N	NA
MIROC6_r1i1p1f1	2.61	1.55	N	N
MIROC-ES2L_r1i1p1f2	2.68	1.55	N	N
MPI-ESM1-2-LR_r1i1p1f1	3.00	1.84	N	N
MRI-ESM2-0_r1i1p1f1	3.15	1.64	N	N
NESM3_r1i1p1f1	4.72	2.72	H	H
NorESM2-LM_r1i1p1f1	2.54	1.48	N	N
NorESM2-MM_r1i1p1f1	2.50	1.33	N	C
TaiESM1_r1i1p1f1	4.31	2.34	H	H

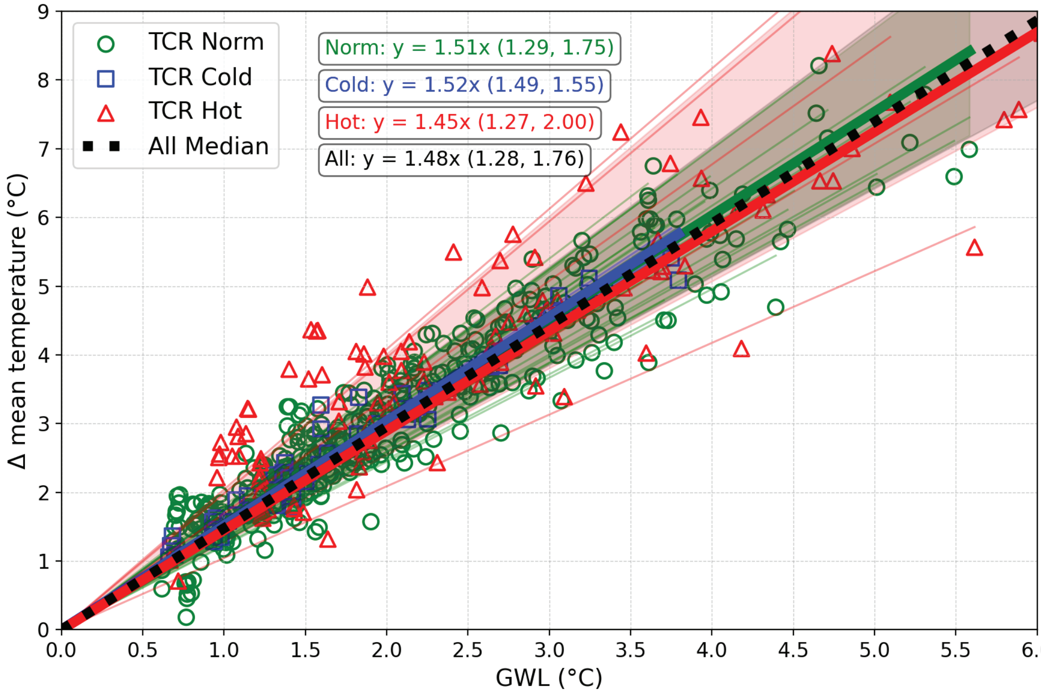

Fig. 1. Relationship between global warming level (GWL) and the change in annual mean temperature over the Estonian land area. Models are categorised as Hot, Cold, or Normal based on their Transient Climate Response (TCR) (see Methods). Each model's trendline is shown in the colour of its category. Bold lines represent the median trend of each category, and shaded areas indicate each group's P10–P90 range.

2021). Applying these criteria retains 21 models (68% of the full ensemble) under the TCR threshold, after excluding two low-sensitivity ("cold") models, seven high-sensitivity ("hot") models, and one model with an unknown TCR value. Under the ECS threshold, 16 models (52%) are retained, following the removal of four cold and eleven hot models. These reduced ensembles are subsequently compared with the full ensemble (Table 1, Fig. 1).

The resulting trends show close agreement across the model groups, as indicated by the similarity of the ensemble median slopes and the substantial overlap of their slope distributions (Fig. 1). This suggests that TCR-based filtering does not lead to meaningful differences in projected regional mean temperature (TG) scaling over Estonia. Similar behavior is found when applying the ECS filter (not shown), and applying both filters also yields nearly identical trends for annual precipitation (not shown). Given the limited subgroup sizes and the lack of strict statistical independence among climate models, we rely on descriptive comparison rather than formal hypothesis testing. As the central tendencies and spreads are highly comparable, we include the full CMIP6 ensemble in our analysis, irrespective of the climate sensitivity of individual models.

Statistical methods

To assess the regional response of Baltic Sea region climate indicators to global warming, we applied a GWL-based approach using CMIP6 model output. Changes in climate indicators were regressed against global mean near-surface air temperature anomalies, both referenced to the pre-industrial baseline (1850–1900). GWLs were calculated using a 20-year running mean of global temperatures. A simulation was considered to reach a given GWL when the midpoint of this smoothed anomaly first equalled or exceeded the respective threshold (e.g., 1.5°C, 2.0°C), consistent with the IPCC AR6 methodology (IPCC 2021).

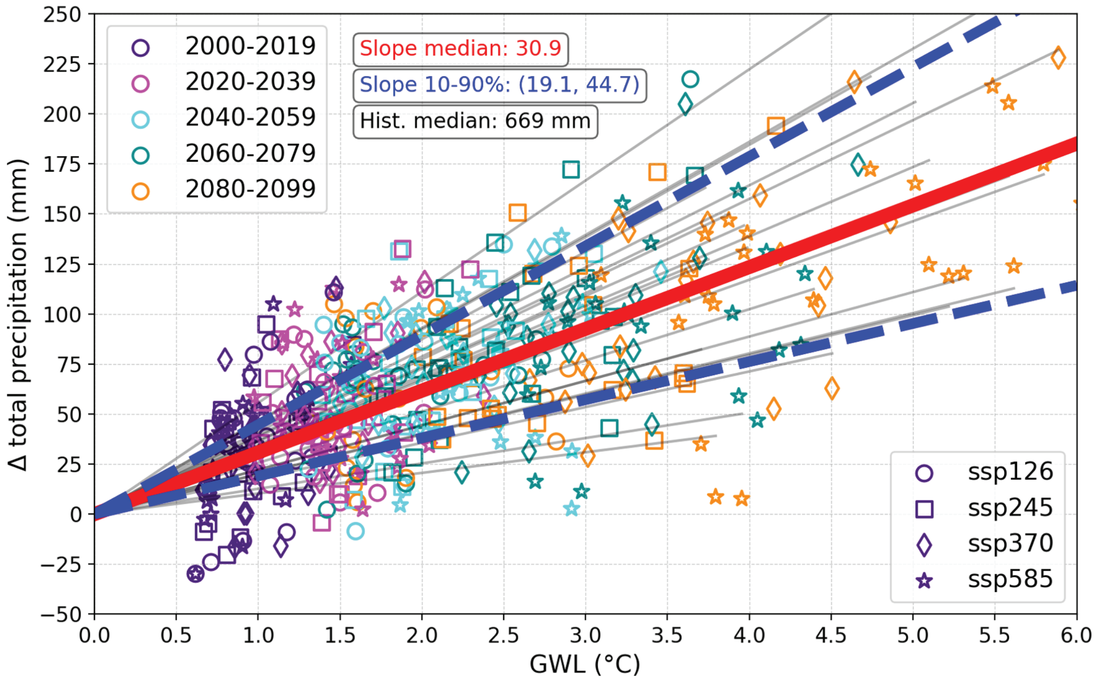

Fig. 2. Relationship between global warming level (GWL) and the change in annual precipitation total over the Estonian land area. Precipitation changes are calculated over consecutive 20-year periods spanning 2000–2099, relative to the historical reference period (1850–1900).

We analysed four Shared Socioeconomic Pathways (SSP) scenarios (SSP1-2.6, SSP2-4.5, SSP3-7.0, and SSP5-8.5), representing the Tier-1 core scenarios in CMIP6 and IPCC AR6 that encompass the full range of plausible future forcing trajectories. Other scenarios (e.g. SSP1-1.9, SSP4-3.4) were excluded due to limited model availability and incomplete temporal coverage. Focusing on these four scenarios ensured consistency across models and enhanced the statistical robustness of the analysis.

Mean indicator values for the spatial mean over the Estonian land area were calculated for five time periods: 2000–2019, 2020–2039, 2040–2059, 2060–2079, and 2080–2099. For each period, the corresponding GWL was determined. For each model, a linear regression without intercept was applied between global temperature anomalies and changes in regional climate indicator values, following Milovac *et al.* (2024). This method assumes no regional change at 0°C of global warming. Each model contributed a single slope per indicator, calculated over all available 20-year periods and SSPs. If all four SSPs (SSP1-2.6, SSP2-4.5, SSP3-7.0, SSP5-8.5) were available, the regression included 20 points (5 time-windows × 4 SSP scenarios) for each climate model, increasing statistical robustness and minimising scenario dependence.

We illustrate the use of the GWL-based approach with annual precipitation as an example (Fig. 2). Each point represents a 20-year mean over Estonia, with colour coding for periods and marker shapes for SSP scenarios. The linear relationship observed across time and scenarios demonstrates the internal consistency within models and supports the use of GWLs for regional climate change assessments. Slopes are calculated separately for each model and then summarised across the ensemble by computing the median trend along with the slope 10th and 90th empirical percentiles, hereafter denoted as P10–P90, representing the central 80% percentile interval. To assess the statistical robustness of projected changes, a signal is considered robust when the entire P10–P90 range has the same sign as the median slope, indicating that at least 90% of models agree on the direction of

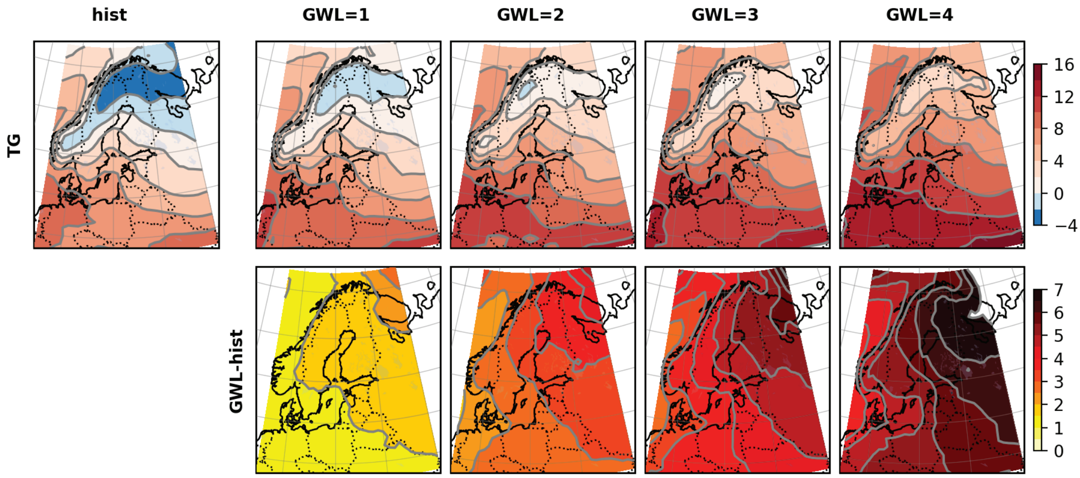

Fig. 3. The first row: The annual mean temperature (°C) of CMIP6 models' median in the Baltic Sea region, depending on the global warming level (GWL). The second row: Change in the annual temperature relative to the historical period (1850–1900).

change. If the P10–P90 interval crosses zero, the projected change is classified as non-robust due to substantial inter-model disagreement. This percentile-based approach provides a distribution-free measure of model agreement and does not assume normality of slope distributions.

Climate indicators were computed using Python libraries icclim v7.0 (Pagé and Aoun 2025) for most indicators. Only for high and low wind days, heating degree days, and heatwave indicators, we used xclim v0.40 (Xclim 2025). Both libraries implement indicator definitions based on the ECA&D methodology (ECA&D Project Team 2013). All indices based on minimum or maximum temperature are computed directly from daily minimum and daily maximum temperature values, respectively. For example, TNn for MAM corresponds to the annual minimum of daily minimum temperatures in spring.

The Estonian land area was defined using the Natural Earth v5.0.0' countries_50' shapefile. To ensure reasonable representation of grid cells partially covering Estonia, the climate indicator data were interpolated to a 0.25° × 0.25° spatial resolution prior to averaging. Interpolated grid cells with more than 50% land coverage within Estonia were included in the spatial mean. For each indicator, spatial averages were computed across these selected grid cells.

Results

Regional temperature-related climate indicators

We defined the Baltic Sea region as a spatial domain spanning 48–72°N and 5–40°E. The warming of the Baltic Sea region in response to global warming is spatially uneven yet strongly dependent on global warming levels, showing clear signs of regional amplification (Fig. 3). This amplification is particularly evident over northeastern areas of the Baltic Sea region. The spatial pattern of warming in the Baltic Sea region is more strongly influenced by the ocean-continent contrast (i.e. continental regions warm faster than ocean regions) than Arctic amplification (high latitudes warm faster). If the global mean temperature increases by 4°C, the regional temperature increases by 4°C to 7°C, indicating up to 1.8-fold amplification – a well-known phenomenon at high latitudes (e.g., Kjellström *et al.* 2018).

In the Estonian land area average, CMIP6 projections indicate a robust warming trend across all seasons and temperature indicators, with a regional temperature response exceeding the global average (Table 2). Based on the CMIP6 ensemble, the annual mean temperature is projected to rise by approximately 1.5°C for every 1°C increase in global mean temperature. The central 80% percentile (P10–P90) range of 1.3–1.8°C $°C^{-1}$ for the slope demonstrates good agreement across models. Winter temperatures show even greater amplification (+1.9°C $°C^{-1}$), while warming is more moderate in summer and autumn (both +1.3°C $°C^{-1}$). The narrow P10–P90 range in the model ensemble highlights high confidence in these projections.

Extremely cold temperatures are projected to diminish substantially, with the annual coldest daily minima (TNn) warming by 3.6°C $°C^{-1}$. This reflects a robust reduction in the severity and frequency of cold extremes. In contrast, hot extremes (TXx) show a more moderate and seasonally variable response, with annual increases of 1.2°C $°C^{-1}$. However, the model spread is wide enough that it remains uncertain whether extremely hot temperatures will increase faster or slower than the global average, underscoring a need for cautious interpretation of these particular indicators. The overall range between annual cold and hot extremes (TXx–TNn) decreases with increasing global temperature across all seasons. The strongest reduction is projected for winter and spring, with reductions ranging from 2.0 to 2.3°C per °C of global warming. Only in summer, the change in range between cold and hot extremes is not statistically robust.

Table 2. CMIP6 models' Estonian land area average temperature-related indicators' annual and seasonal medians for the historical period 1850–1900, the median regression slope *K* (change in the indicator per 1°C of global warming), and the central 80% model range (P10–P90) interval for *K*. All presented slopes are statistically robust as P10–P90 does not cross zero.

Code	Climate indicator	Unit	Period	Med	K_{med}	$K_{10\%}$	$K_{90\%}$
TG	Mean temperature	(°C)	YEAR	3.7	1.5	1.3	1.8
TG	Mean temperature	(°C)	DJF	–8.1	1.9	1.6	2.5
TG	Mean temperature	(°C)	MAM	2.1	1.5	1.2	1.9
TG	Mean temperature	(°C)	JJA	15.1	1.3	1.1	1.6
TG	Mean temperature	(°C)	SON	5.2	1.3	1.1	1.6
TNn	Min of daily min temperature	(°C)	YEAR	–25.4	3.6	2.8	4.8
TNn	Min of daily min temperature	(°C)	DJF	–24.8	3.6	2.8	4.8
TNn	Min of daily min temperature	(°C)	MAM	–18.4	3.0	2.3	4.4
TNn	Min of daily min temperature	(°C)	JJA	4.8	1.3	1.0	1.7
TNn	Min of daily min temperature	(°C)	SON	–10.6	2.1	1.5	3.7
TXx	Max of daily max temperature	(°C)	YEAR	26.4	1.2	0.9	2.3
TXx	Max of daily max temperature	(°C)	DJF	4.1	1.3	1.0	1.5
TXx	Max of daily max temperature	(°C)	MAM	19.9	1.0	0.8	1.6
TXx	Max of daily max temperature	(°C)	JJA	26.4	1.2	0.9	2.3
TXx	Max of daily max temperature	(°C)	SON	19.6	1.3	0.9	2.1
TX10p	Cool days (TX<10%)	%	YEAR	9.4	–3.2	–4.1	–2.2
TX90p	Warm days (TX>90%)	%	YEAR	10.8	9.9	7.0	13.2
TN10p	Cool nights (TN<10%)	%	YEAR	8.9	–3.0	–4.1	–2.0
TN90p	Warm nights (TN>90%)	%	YEAR	11.0	11.0	7.0	13.0
FD	Frost days (TN<0 °C)	days	YEAR	156.0	–20.0	–26.0	–15.0
CFD	Max nr of consec. frost days	days	YEAR	70.0	–14.0	–19.0	–7.0
SU	Summer days (TX>25 °C)	days	YEAR	4.9	6.4	1.6	11.8
CSU	Max nr of consec. summer days	days	YEAR	2.1	2.0	0.7	4.4
HD17	Heating degree days	°C days	YEAR	4856.0	–469.0	–610.0	–398.0
CDD18	Cooling degree days	°C days	YEAR	36.0	45.0	20.0	87.0
ID	Ice days (TX<0 °C)	days	YEAR	97	–15	–20	–13
TR	Tropical nights (TN>20 °C)	days	YEAR	0.2	1.5	0.2	5.8
GSL	Growing season length	days	YEAR	175	14.4	11.1	16.6
HWML	Heat wave max length	days	YEAR	1.1	1.4	0.7	3.4
HWTL	Heat wave total length	days	YEAR	1.5	3.2	1.2	9.8
HWF	Heat wave frequency	counts/year	YEAR	0.3	0.5	0.2	0.9

Indicators associated with cold half-year climate conditions consistently show strong declines. Frost days (FD: count of days when min of daily temperature < 0°C), ice days (ID: count of days when max of daily temperature < 0°C), and heating degree days (HD17: sum over difference between 17°C and the daily mean temperature for all days when the daily mean temperature is below 17°C) are all expected to decrease robustly with warming (Table 2). There will be 20 (13%) frost days and nearly 500°C days (10%) fewer heating degree days with each degree of global warming. These trends imply a notable reduction in cold-related health risks, energy demand, and stress on infrastructure. Similarly, the number of consecutive frost days (CFD) is expected to decline by 14 days (20%) per°C of global warming, suggesting fewer and shorter sequences of sub-freezing periods.

Conversely, heat-related climate indicators, associated with the warm half-year, exhibit a consistent increase. Summer days (SU: count of days when the daily maximum temperature > 25°C), tropical nights (TR: count of days when the daily minimum temperature > 20°C) and cooling degree days (CDD18: sum over difference between 18°C and the daily mean temperature for all days when the daily mean temperature exceeds 18°C) have historically been rare in Estonia. These indicators are projected to increase notably, although their projected rates of change vary considerably across the model ensemble. The P10–P90 range of modelled increases per degree of global warming spans 1.6–11.8 days for SU, 0.2–5.8 days for TR and 20–87°C days for CDD18 (Table 2). The projected emergence and intensification of these events point to a fundamental shift in Estonia's warm-season climate characteristics. The frequency and duration of heatwaves are also projected to increase across all models. Indicators such as heatwave maximum length (HWML), heatwave total length (HWTL), and heatwave frequency (HWF; see ECA&D Project Team 2013 for definitions) all show positive and statistically robust trends per°C of global warming (Table 2), confirming an intensification of extreme heat events.

Regional precipitation-related climate indicators

Projected precipitation changes over the Baltic Sea region show strong spatial variability and seasonally variable responses to global warming (Fig. 4). Total annual precipitation is expected to increase across most of the region, particularly near the Atlantic coast of Scandinavia. The largest increases are projected for western and northern Norway, especially in orographic zones exposed to moist westerly airflows, where annual precipitation is up to 1800 mm and increases by up to 300 mm (17%) at GWL = 4. More moderate increases are projected across inland Scandinavia, while southern and south-eastern areas exhibit smaller and less robust changes.

Although most of the study area shows an annual increase in precipitation, the southernmost regions show a decrease of up to 30 mm at GWL = 4. This annual reduction is primarily driven by summer conditions, when large parts of the land area south of 60°N exhibit declining precipitation (not shown). In addition, parts of the southern region show also decreases in autumn. This north–south contrast reflects the intensification of the atmospheric water cycle, with wetter northern areas becoming wetter and drier southern areas becoming drier (IPCC 2021: WGI Ch. 8). No decreases are projected for winter or spring across the study domain (not shown).

In Estonia, annual precipitation totals are projected to rise in line with broader regional trends, with models showing agreement on both direction and magnitude of change (Table 3). According to the CMIP6 ensemble, annual total precipitation (PRCPTOT) is expected to increase by approximately 31 mm (4.6%) per 1°C of global warming. The relatively narrow P10–P90 model spread suggests high confidence in this overall increase.

Seasonal precipitation projections for Estonia show the most substantial increases in winter and autumn, with winter precipitation rising by 13 mm $°C^{-1}$ (8.6% $°C^{-1}$) and autumn by 9 mm $°C^{-1}$ (4.6% $°C^{-1}$). These results are supported by consistent trends across models, indicating robust seasonal responses. Springtime precipitation also increases (7 mm $°C^{-1}$ or about

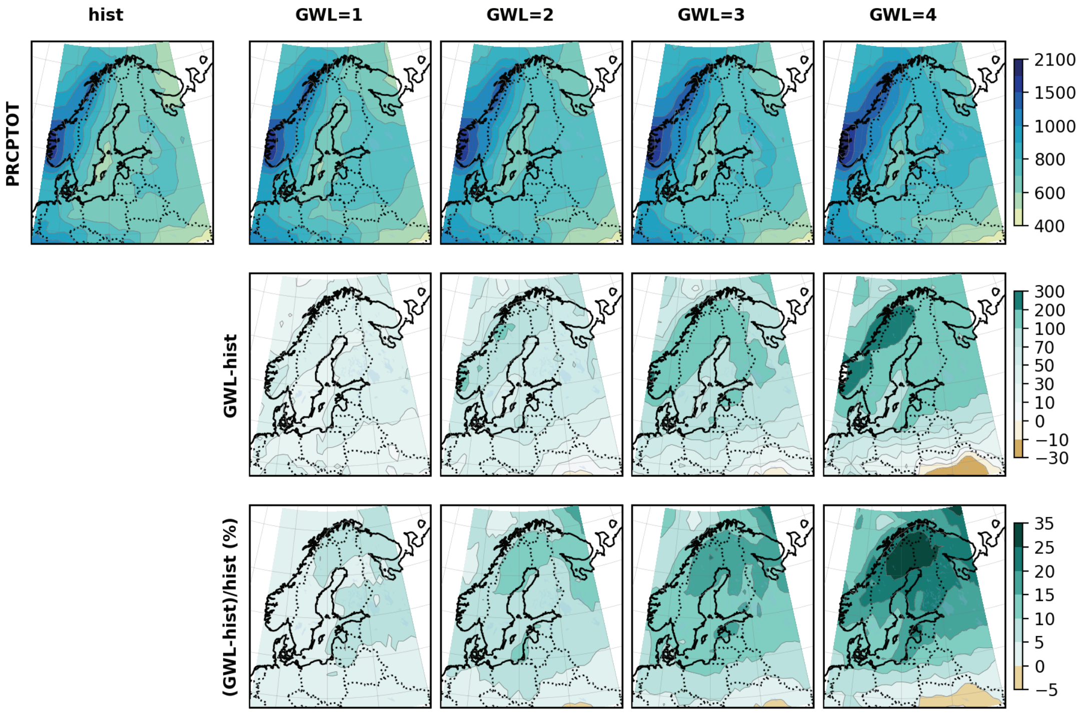

Fig. 4. First row: The annual precipitation (mm year^{-1}) over the Baltic Sea region depending on the global warming level (GWL). Second row: Change in the annual precipitation relative to the historical period (1850–1900). Third row: Relative change (%) in annual precipitation relative to the historical period.

5.0% °C^{-1}), though slightly less than in the cold seasons. In contrast, projections for the summer are highly uncertain and not robust: the projected increase is only 1 mm °C^{-1} (0.6% °C^{-1}), and the P10–P90 range is from –8 mm °C^{-1} to 14 mm °C^{-1} (–5 to +8% °C^{-1}), indicating vast variance between models' projections. The negative P10 is consistent with the broader summer projection pattern across the study area, where in most of the land areas south of 60°N, precipitation decreases (not shown).

The number of wet days (RR1: days when daily precipitation amount > 1.0 mm) is projected to slightly increase overall, with a change of 1.6 days per°C of global warming. However, this signal is not robust, as more than 10% of the models indicate a decrease in the number of wet days. There are relatively robust increases in winter and spring, while changes in summer and autumn are smaller and less consistent. In summer, more than half of the models project a decline in the number of wet days, further highlighting the uncertainty of warm-season precipitation changes in Estonia. The simple precipitation intensity index (SDII) shows a steady increase (+0.16 mm (wet day)$^{-1}$ °C^{-1}), supported by tight inter-model ranges.

Extreme precipitation events intensify more clearly and consistently than total precipitation. Both the maximum 1-day (RX1day) and 5-day (RX5day) precipitation show robust increases, with +1.3 mm °C^{-1} and +2.4 mm °C^{-1}, respectively, corresponding to an approximate 5% rise for both. The frequency of heavy and very heavy rainfall days is also projected to increase. The number of days with more than 10 mm of precipitation (R10mm) increases by 1.5 days °C^{-1}, while days with more than 20 mm (R20mm) increase by 0.3 days °C^{-1}. Although these changes may appear small in absolute terms, they represent notable relative increases — approximately 13% for R10mm and 25% for R20mm. The projected increases are consistent across models and seasons (not shown).

Changes in the duration of wet and dry spells show higher model disagreement and weaker trends. The annual maximum number of consecutive wet days (CWD) is projected to increase slightly (+0.18 days °C^{-1}), with the most robust increases in winter and spring (not shown). However, changes in summer and autumn are minimal and not statistically significant (not shown). Meanwhile, the annual maximum number of consecutive dry days (CDD) shows no robust trend. Its P10–P90 range spans both positive and negative values (–0.5 to +0.6 days °C^{-1}), reflecting substantial model disagreement. Only winter shows a statistically robust decrease in CDD, while projected summer increases remain uncertain (not shown).

In addition, we examined changes in evaporation (EVG). Annual evaporation is projected to increase at an average rate of 27 mm °C^{-1} (6% °C^{-1}), with high inter-model agreement. Although the median annual precipitation increase exceeds that of evaporation, evaporation tends to increase faster than precipitation in summer and spring.

Regional wind-related climate indicators

Projected changes in wind speed over the Baltic Sea region under increasing GWLs indicate a generally weak and spatially inconsistent response, with a slight trend toward decreasing mean wind speeds (Fig. 5). In Estonia, CMIP6 projections show a small decline in annual mean wind speed (FG), with a median change of −0.04 m s^{-1} °C^{-1} of global warming (Table 4). However, the inter-model range spans from −0.18 to +0.01 m s^{-1} °C^{-1}, indicating that the annual trend is not statistically robust.

Table 3. CMIP6 models' Estonian land area average precipitation-related indicators' annual and seasonal medians for the historical period 1850–1900, the median regression slope *K* (change in the indicator per 1°C of global warming), and the central 80% model range (P10–P90) for *K*. Slopes are considered statistically robust when the P10– P90 interval does not cross zero; non-robust slopes are indicated by an asterisk (*).

Code	Climate indicator	Unit	Period	Med	K_{med}	$K_{10\%}$	$K_{90\%}$
PRCPTOT	Total precipitation	mm	YEAR	669	31	19	45
PRCPTOT	Total precipitation	mm	DJF	152	13	6	18
PRCPTOT	Total precipitation	mm	MAM	139	7	5	12
PRCPTOT	Total precipitation	mm	JJA	177	1*	–8	14
PRCPTOT	Total precipitation	mm	SON	196	9	4	12
RR1	Wet days	days	YEAR	144	1.6*	–0.9	4.0
RR1	Wet days	days	DJF	37.9	1.7	0.5	2.3
RR1	Wet days	days	MAM	30.2	0.7	0.2	1.6
RR1	Wet days	days	JJA	35.4	–0.4*	–2.6	1.2
RR1	Wet days	days	SON	39.9	0.2*	–0.4	1.1
RX1day	Highest 1-day precip. amount	mm	YEAR	23.5	1.3	0.9	2.1
RX5day	Highest 5-day precip. amount	mm	YEAR	46.0	2.4	1.5	3.8
SDII	Simple daily intensity index	mm/wet days	YEAR	4.22	0.16	0.12	0.21
R10mm	Heavy precipitation days (RR >10 mm)	days	YEAR	11.1	1.5	1.1	2.0
R20mm	Very heavy precipitation days (RR > 20 mm)	days	YEAR	1.19	0.30	0.15	0.43
CWD	Maximum no of consec. wet days	days	YEAR	9.55	0.18	0.06	0.52
CDD	Maximum no of consec. dry days	days	YEAR	19.7	0.0*	–0.5	0.6
SPI3	3-Month Standardized Precip. Index	—	YEAR	0.00	0.11	0.07	0.16
SPI6	6-Month Standardized Precip. Index	—	YEAR	0.00	0.14	0.09	0.22
EVG	Total evaporation	mm	YEAR	452	27	16	41
EVG	Total evaporation	mm	DJF	27	5	3	9
EVG	Total evaporation	mm	MAM	97	9	5	13
EVG	Total evaporation	mm	JJA	228	7	1	13
EVG	Total evaporation	mm	SON	102	5	3	9

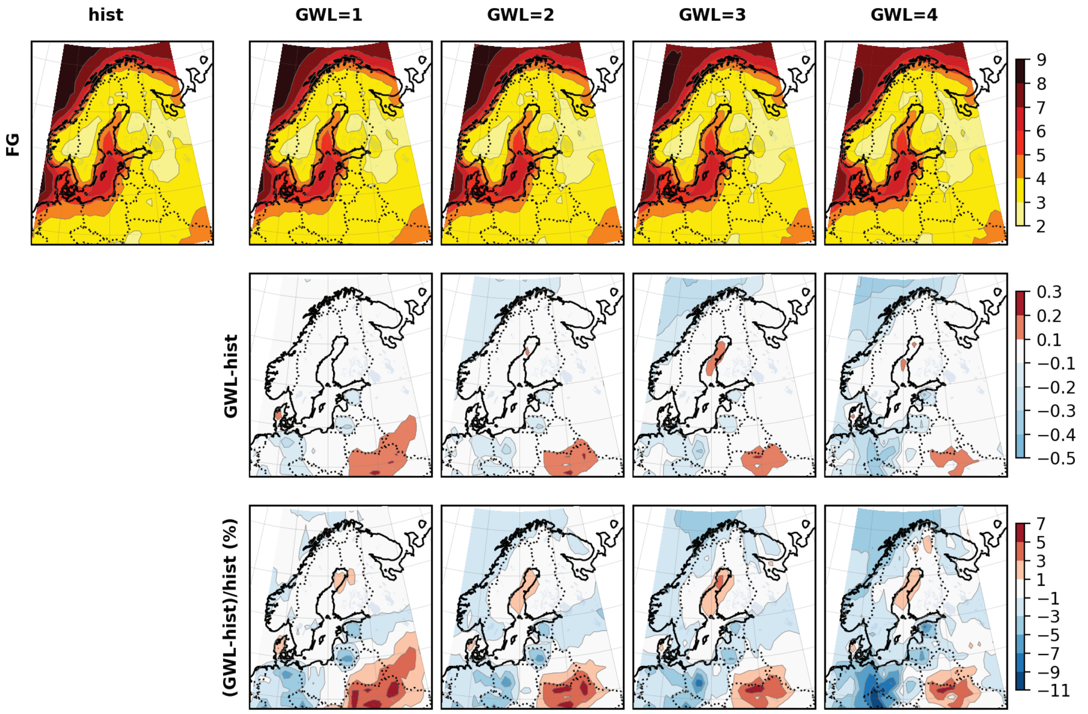

Fig. 5. First row: The annual wind speed (m s^{-1}) over the Baltic Sea region depending on the global warming level (GWL). Second row: Change in the annual wind speed relative to the historical period (1850–1900). Third row: Relative change (%) in annual wind speed relative to the historical period.

In all seasons, most models project decreasing wind speeds, but the consistency of the signal varies. Summer (JJA) shows the clearest decline (−0.09 m s^{-1} °C^{-1}), with the P10–P90 range entirely below zero, indicating a consistent decrease across models. In other seasons, the upper bound of the P10–P90 range reaches from 0.00 m s^{-1} °C^{-1} in autumn to 0.05 m s^{-1} °C^{-1} in winter, suggesting that the wind speed trend is close to, but not fully robust. Substantial inter-model disagreement indicates the possibility of both increases and decreases in wind speeds.

Indicators of wind speed extremes show weak and inconsistent responses. The number of low-wind days (LWD: number of days with average wind speed < 2 m s^{-1}) is projected to increase slightly (by 2.0 days °C^{-1}) from a historical median of 34 days per year. However, the

Table 4. CMIP6 models' Estonian land area average wind-related indicators' annual and seasonal medians for the historical period 1850–1900, the median regression slope *K* (change in the indicator per 1°C of global warming), and the central 80% model range (P10–P90) for *K*. Slopes are considered statistically robust when the P10–P90 interval does not cross zero; non-robust slopes are indicated by an asterisk (*).

Code	Climate indicator	Unit	Period	Med	K_{med}	$K_{10\%}$	$K_{90\%}$
FG	Mean wind speed	m/s	YEAR	3.79	–0.04*	–0.18	0.01
FG	Mean wind speed	m/s	DJF	4.36	–0.01*	–0.17	0.05
FG	Mean wind speed	m/s	MAM	3.49	–0.02*	–0.16	0.02
FG	Mean wind speed	m/s	JJA	3.27	–0.09	–0.18	–0.01
FG	Mean wind speed	m/s	SON	4.04	–0.06	–0.18	0.00
LWD	Low wind days (FG < 2 m/s)	days	YEAR	34.4	2.0*	–0.6	7.2
HWD	High wind days (FG > 10.8 m/s)	days	YEAR	2.33	0.02*	–0.07	0.07

large P10–P90 range (−0.6 to +7.2 days °C^{-1}) reflects high variability between models and a lack of statistical robustness. Similarly, high-wind days (HWD: number of days with average wind speed > 10.8 m s^{-1}) are projected to remain nearly unchanged, with a median change of +0.02 days °C^{-1} and a model spread from −0.07 to +0.07 days °C^{-1}, indicating no consistent signal under warming.

Discussion and conclusions

We used a GWL-based approach to assess the scalability of climate change in Estonia with global warming using CMIP6 climate model projections. Temperature-related changes in Estonia exhibit high model agreement across all seasons and indicators, reflecting the dominance of thermodynamic controls: warming robustly scales with the accumulation of greenhouse gases in the atmosphere and radiative forcing. Annual mean temperature increases by approximately 1.5°C per 1°C of global warming, with stronger amplification in winter (+1.9°C °C^{-1}) and weaker in summer (+1.3°C °C^{-1}). This seasonal amplification pattern is consistent with Arctic and sub-Arctic amplification of warming (IPCC 2021: WGI Ch4).

The projected warming is accompanied by a pronounced reduction in cold extremes, including the coldest daily minimum temperature, the number of frost days, ice days, heating degree days, and the number of consecutive frost days. These declines indicate a substantial reduction in cold-season severity. Conversely, warm-season indicators show consistent increases. These include the hottest daily maximum temperature, the number of summer days and tropical nights, cooling degree days, and also heatwave-related metrics. The emergence of tropical nights and the intensification of heatwaves indicate a qualitative shift in Estonia's warm-season climate, with potential implications for human health, agriculture, and energy demand.

Evaporation also shows robust increases across all seasons, reflecting its strong physical linkage to temperature through saturation vapour pressure and availability of energy for evaporation. Projected increases in evaporation are consistent with the intensification of the atmospheric water cycle under warming (IPCC 2021: WGI Ch. 8) and contribute to increasing summer soil moisture deficits, particularly given the uncertainty in summer precipitation trends.

Annual and cold-season precipitation totals are projected to increase with high confidence, consistent with intensification of the atmospheric water cycle (IPCC 2021: WGI Ch. 8). In contrast, summer precipitation shows weak and non-robust changes, with more than one-quarter of models projecting decreases. This summer pattern aligns with the possible regional drying pattern south of 60° N. While the change in total summer precipitation remains uncertain, extreme precipitation indicators show robust increases.

In fact, extreme precipitation indicators show robust increases across all seasons. This is consistent with conclusions that heavy precipitation intensity is projected to increase almost everywhere due to thermodynamic enhancement of moisture availability, even in regions where mean precipitation declines (IPCC 2021: SPM and WGI Ch. 11). Here, extreme precipitation indicators include the maximum 1-day precipitation amount, the maximum consecutive 5-day precipitation amount, and the number of days with heavy and very heavy precipitation. In the Baltic Sea region, there are narrow inter-model spreads for indicators of extreme precipitation, suggesting high confidence in the intensification of short-duration heavy rainfall events. Projected increases in extreme precipitation indicators imply heightened risks of short-duration high-intensity rainfall events, even in seasons without clear changes in total precipitation. Moreover, the expected rise in hydroclimate volatility — rapid shifts between very wet and very dry conditions – further amplifies these risks, particularly under continued warming (Swain *et al*. 2025).

Stronger evaporation may offset precipitation increases, especially in summer and spring, leading to drier soils, reduced water availability for vegetation, and increased agricultural drought risk (IPCC 2021: AR6 Ch8). It may also intensify heat stress through land-atmosphere feedbacks, as reduced soil moisture limits evaporative cooling (Miralles *et al*. 2018). Consequently, despite an increase in annual mean wetness, seasonal water availability may become more variable, with heightened summer dryness and increased pressure on ecosystems and water management systems (Swain *et al*. 2025).

While precipitation responses are driven by both thermodynamic and dynamic influences, changes in winds in the Baltic Sea region are largely driven by circulation responses to global warming (Christensen and Kjellström 2018). Owing to the dynamic drivers, wind speed projections exhibit the weakest and least spatially consistent changes. We detected modest but robust declines only in summer mean wind speeds over Estonia. These patterns align with AR6 findings that changes in circulation-dependent variables such as wind speed are subject to larger uncertainties due to model spread in atmospheric circulation responses to global warming (IPCC 2021: WGI Ch. 4 and 8).

Moreover, in addition to forced circulation responses, inter-model spread could be explained by unforced internal climate variability and climate model formulations (Hawkins and Sutton 2009, Deser and Phillips 2023). The differences in horizontal resolutions between climate models can explain part of the model spread, e.g. this has been clearly shown for precipitation distributions (Strandberg and Lind 2021, Liu *et al.* 2025). In addition, different physical parameterizations can lead to model spread, as has been demonstrated by testing various parameterizations within the same model for regional climate model simulations over Europe (García-Díez *et al.* 2015). Finally, differences in spatial patterns of radiative forcing across climate models could explain part of the model spread (Shindell *et al.* 2015).

Overall, the high confidence in temperature and extreme precipitation projections is rooted in the thermodynamic control consistently represented across models, while the greater uncertainty in summer precipitation and wind speeds reflects their dependence on uncertain circulation responses. While in this research we have scaled the most robust regional climate responses in Estonia on global warming levels, future research should add circulation responses as an extra dimension. To describe regional climate change in the Baltic Sea region in more detail, we suggest adding storylines of large-scale atmospheric circulation responses (Zappa and Shepherd 2017, Shepherd *et al.* 2018, Shepherd 2019, Zappa 2019) on top of the GWL-based approach. For this, lower, medium and higher levels of global warming can be combined with increased/reduced cyclonic activity or specific relevant drivers of large-scale circulation responses, like polar and tropical amplification of global warming and changes in the strength of the stratospheric vortex, following Zappa and Shepherd (2017). This could help to separate the contribution of forced circulation responses in inter-model spread in the Baltic Sea region from the other contributors to the inter-model spread, like unforced internal climate variability and structural differences between climate models (Hawkins and Sutton 2009, Deser and Phillips 2023, García-Díez *et al.* 2015).

Acknowledgements: The work was funded by the project "Implementation of national climate change adaptation activities in Estonia" (LIFE21-IPC-EE-LIFE-SIP AdaptEst/101069566), which is supported by the environmental projects' co-funded programme LIFE of the Member States of the European Union, and the Estonian state from the revenues of trading greenhouse gas emission allowances. Neither the European Union nor the granting authorities are responsible for the accuracy and use of the information contained in the research. We acknowledge the use of the icclim and xclim Python libraries, which provide tools for computing climate indices. We acknowledge the Amazon Web Services (AWS) Open Data Program for providing access to the CMIP6 data. We also thank the anonymous reviewer for their careful reading of the manuscript and highly constructive comments, which significantly improved the clarity and robustness of this study.

Code availability: The analysis scripts used in this study are available in the GitLab repository and have been archived on Zenodo: Jakobson *et al.* (2026) https://doi.org/10.5281/zenodo.20059032.

References

Amazon Web Services (AWS) Open Data Program 2025. Coupled Model Intercomparison Project Phase 6 (CMIP6) data hosted on AWS. Available at: https://registry.opendata.aws/cmip6/ [accessed 28 May 2025].

Becsi B. & Formayer H. 2024. Linking local climate scenarios to global warming levels: applicability, prospects and uncertainties. *Environmental Research: Climate* 3, 045003, https://doi.org/10.1088/2752-5295/ad574e.

Christensen O.B. & Kjellström E. 2018. Projections for temperature, precipitation, wind, and snow in the Baltic Sea region until 2100. *Oxford Research Encyclopedia of Climate Science*, https://doi.org/10.1093/acrefore/9780190228620.013.695.

Cradock-Henry N.A., Blackett P., Hall M., Johnstone P., Teixeira E. & Wreford A. 2020. Climate adaptation pathways for agriculture: insights from a participatory process. *Environmental Science and Policy* 107: 66–79, https://doi.org/10.1016/j.envsci.2020.02.020.

CSIC 2023. Copernicus Interactive Climate Atlas (C3S Atlas). *Copernicus Climate Change Service*, https://atlas.climate.copernicus.eu/atlas.

Da Silva N.A. & Haerter J.O. 2025. Super-Clausius-Clapeyron scaling of extreme precipitation explained by shift from stratiform to convective rain type. *Nature Geoscience* 18(5): 382–388, https://doi.org/10.1038/s41561-025-01686-4.

Deser C. & Phillips A.S. 2023. A range of outcomes: the combined effects of internal variability and anthropogenic forcing on regional climate trends over Europe. *Nonlinear Processes in Geophysics* 30: 63–84, https://doi.org/10.5194/npg-30-63-2023.

ECA&D Project Team 2013. European Climate Assessment & Dataset (ECA&D) Algorithm Theoretical Basis Document (ATBD), Version 10.7. Royal Netherlands Meteorological Institute (KNMI), De Bilt, The Netherlands. EUMETNET/ECSN optional programme. Project number: EPJ029135. Available at: https://www.ecad.eu/documents/atbd.pdf [accessed 28 July 2025].

Eyring V., Bony S., Meehl G.A., Senior C.A., Stevens B., Stouffer R.J. & Taylor K.E. 2016. Overview of the Coupled Model Intercomparison Project Phase 6 (CMIP6) experimental design and organisation. *Geoscientific Model Development* 9(5): 1937–1958, https://doi.org/10.5194/gmd-9-1937-2016.

García-Díez M., Fernández J. & Vautard R. 2015. An RCM multi-physics ensemble over Europe: multi-variable evaluation to avoid error compensation. *Climate Dynamics* 45: 3141–3156, https://doi.org/10.1007/s00382-015-2529-x.

Goldenson N., Leung L.R., Mearns L.O., Pierce D.W., Reed K.A., Simpson I.R., Ullrich P., Krantz W., Hall A., Jones A. & Rahimi S. 2023. Use-inspired, process-oriented GCM selection: prioritising models for regional dynamical downscaling. *Bulletin of the American Meteorological Society* 104: E1619–E1629, https://doi.org/10.1175/BAMS-D-23-0100.1.

Hausfather Z., Marvel K., Schmidt G.A., Nielsen-Gammon J.W. & Zelinka M. 2022. Climate simulations: recognise the “hot model” problem. *Nature* 605(7908): 26–29, https://doi.org/10.1038/d41586-022-01192-2.

Hawkins E. & Sutton R. 2009. The potential to narrow uncertainty in regional climate predictions. *Bulletin of the American Meteorological Society* 90: 1095–1108, https://doi.org/10.1175/2009BAMS2607.1.

Intergovernmental Panel on Climate Change (IPCC) 2021. *Climate change 2021: the physical science basis. Contribution of Working Group I to the Sixth Assessment Report of the Intergovernmental Panel on Climate Change*, edited by V. Masson-Delmotte, P. Zhai, A. Pirani *et al.*, Cambridge University Press, Cambridge, U.K.

Jakobson E., Luhamaa A., Keernik H., Jakobson L., Toll V., Post P. & Aun M. 2026. Scalability of climate change in Estonia with the level of global warming (v1.0.0). *Zenodo*, https://doi.org/10.5281/zenodo.20059032.

Kjellström E., Nikulin G., Strandberg G., Christensen O.B., Jacob D., Keuler K., Lenderink G., Meijgaard E., Schär C., Somot S., Sørland S.L., Teichmann C. & Vautard R. 2018. European climate change at global mean temperature increases of 1.5 and 2 °C above pre-industrial conditions as simulated by the EURO-CORDEX regional climate models. *Earth System Dynamics* 9(2): 459–478, https://doi.org/10.5194/esd-9-459-2018.

Lafferty D.C. & Sriver R.L. 2023. Downscaling and bias-correction contribute considerable uncertainty to local climate projections in CMIP6. *npj Climate and Atmospheric Science* 6(1): 1–13, https://doi.org/10.1038/s41612-023-00486-0.

Liu Y., Kjellsson J., Savita A. & Park W. 2025. Impact of horizontal resolution and model time step on European precipitation extremes in the OpenIFS 43r3 atmospheric model. *Geoscientific Model Development* 18: 5435–5449, https://doi.org/10.5194/gmd-18-5435-2025.

Milovac J., Iturbide M., Fernández J., Gutiérrez J.M., Diez-Sierra J. & Jones R.G. 2024. Regional scaling of sea surface temperature with global warming levels in the CMIP6 ensemble. *Climate Dynamics* 62(7): 6447–6465, https://doi.org/10.1007/s00382-024-07218-x.

Miralles D.G., Gentine P., Seneviratne S.I. & Teuling A.J. 2018. Land-atmospheric feedbacks during droughts and heatwaves: state of the science and current challenges. *Annals of the New York Academy of Sciences* 1436(1): 19–35, https://doi.org/10.1111/nyas.13912.

Pagé C. & Aoun A. 2025. Icclim: Python library for climate indices calculation. Available at: https://icclim.readthedocs.io/ [accessed 28 May 2025].

Palmer T.E., McSweeney C.E., Booth B.B.B., Priestley M.D.K., Davini P., Brunner L., Borchert L. & Menary M.B. 2023. Performance-based sub-selection of CMIP6 models for impact assessments in Europe. *Earth System Dynamics* 14(2): 457–483, https://doi.org/10.5194/esd-14-457-2023.

Ruosteenoja K. & Jylhä K. 2025. Extreme cold days and spells in northern Europe at 0.5°C–2.0°C global warming levels. *International Journal of Climatology* 45, e8875, https://doi.org/10.1002/joc.8875.

Shepherd T. 2014. Atmospheric circulation as a source of uncertainty in climate change projections. *Nature Geoscience* 7: 703–708, https://doi.org/10.1038/ngeo2253.

Shepherd T.G., Boyd E., Calel R.A., Chapman S.C., Dessai S., Dima-West I.M., Fowler H.J., James R., Maraun D., Martius O., Senior C.A., Sobel A.H., Stainforth D.A., Tett S.F.B., Trenberth K.E., van den Hurk B.J.J.M., Watkins N.W., Wilby R.L. & Zenghelis D.A. 2018. Storylines: an alternative approach to representing uncertainty in physical aspects of climate change. *Climatic Change* 151: 555–571, https://doi.org/10.1007/

s10584-018-2317-9.

Shepherd T.G. 2019. Storyline approach to the construction of regional climate change information. *Proceedings of the Royal Society A* 475, 20190013, https://doi.org/10.1098/rspa.2019.0013.

Shindell D.T., Faluvegi G., Rotstayn L. & Milly G. 2015. Spatial patterns of radiative forcing and surface temperature response. *Journal of Geophysical Research: Atmospheres* 120: 5385–5403, https://doi.org/10.1002/2014JD022752.

Smith C., Nicholls Z.R.J., Armour K., Collins W., Forster P., Meinshausen M., Palmer M.D. & Watanabe M. 2021. The Earth's energy budget, climate feedbacks, and climate sensitivity supplementary material. In: *Climate change 2021: the physical science basis*, IPCC AR6 WG1, https://www.ipcc.ch/.

Snyder A., Prime N., Tebaldi C. & Dorheim K. 2024. Uncertainty-informed selection of CMIP6 Earth system model subsets for use in multisectoral and impact models. *Earth System Dynamics* 15(5): 1301–1318, https://doi.org/10.5194/esd-15-1301-2024.

Stammer D., Bracco A., Braconnot P., Brasseur G.P., Griffies S.M. & Hawkins E. 2018. Science directions in a post COP21 world of transient climate change: enabling regional to local predictions in support of reliable climate information. *Earth's Future* 6(11): 1498–1507, https://doi.org/10.1029/2018EF000979.

Strandberg G. & Lind P. 2021. The importance of horizontal model resolution on simulated precipitation in Europe – from global to regional models. *Weather and Climate Dynamics* 2: 181–204, https://doi.org/10.5194/wcd-2-181-2021.

Swain D.L., Prein A.F., Abatzoglou J.T., Albano C.M., Brunner M., Diffenbaugh N.S., Singh D., Skinner C.B. & Touma D. 2025. Hydroclimate volatility on a warming Earth. *Nature Reviews Earth and Environment* 6: 35–50, https://doi.org/10.1038/s43017-024-00624-z.

Xclim 2025. Xclim: Python library for climate indicators. Available at: https://xclim.readthedocs.io/ [accessed 28 May 2025].

Zappa G. 2019. Regional climate impacts of future changes in the mid-latitude atmospheric circulation: a storyline view. *Current Climate Change Reports* 5: 358–371, https://doi.org/10.1007/s40641-019-00146-7.

Zappa G. & Shepherd T.G. 2017. Storylines of atmospheric circulation change for European regional climate impact assessment. *Journal of Climate* 30: 6561–6577, https://doi.org/10.1175/JCLI-D-16-0807.1.